

# 黔南马坡脚上二叠统吴家坪组凝灰岩成因及其地质意义

杨晨晨<sup>1</sup>, 黄虎<sup>1\*</sup>, 邓昌州<sup>2</sup>

1. 成都理工大学 沉积地质研究院, 成都 610059;  
2. 中国科学院 地球化学研究所, 矿床地球化学国家重点实验室, 贵阳 550081

**摘要:**为确定贵州南部马坡脚上二叠统海相碳酸盐岩夹凝灰岩的形成年代、成因及其与峨眉山大火成岩省的关系, 对其进行了全岩地球化学、锆石 U-Pb 年龄、锆石微量元素及 Hf 同位素分析。结果显示, 马坡脚凝灰岩具有较高的  $\text{Al}_2\text{O}_3/\text{TiO}_2$  比值和显著的 Eu 负异常。2 个样品的锆石 U-Pb 年龄分别为  $(259.1 \pm 1.5)$  Ma 和  $(257.5 \pm 1.8)$  Ma, 与云南宾川酸性熔结凝灰岩的年龄相近。马坡脚凝灰岩中锆石的  $\varepsilon_{\text{Hf}}(t)$  值为  $+1.1 \sim +8.4$ , 且 Th/Nb 比值较低, 具有板内岩浆岩的地球化学性质。锆石年龄和地球化学特征指示马坡脚凝灰岩可能来自峨眉山大火成岩省的酸性火山活动。结合已发表的高精度 CA-TIMS 年龄与牙形石生物地层年龄, 可以认为峨眉山酸性火山活动可能至少持续至晚二叠世吴家坪早期, 且峨眉山酸性火山喷发可能是导致吴家坪期气候变冷的重要影响因素之一。

**关键词:**凝灰岩; 地球化学; 锆石 U-Pb 年龄; Hf 同位素; 峨眉山大火成岩省; 气候变冷

中图分类号:P588.12<sup>+</sup>1 文章编号:1007-2802(2022)02-0397-17 doi:10.19658/j.issn.1007-2802.2022.41.009

## The Origin and Geologic Significance of the Tuff within the Upper Permian Wuchiaping Formation at Mapojiao in the Southern Guizhou, China

YANG Chen-chen<sup>1</sup>, HUANG Hu<sup>1\*</sup>, DENG Chang-zhou<sup>2</sup>

1. Institute of Sedimentary Geology, Chengdu University of Technology, Chengdu 610059, China; 2. State Key Laboratory of Ore Deposit Geochemistry, Institute of Geochemistry, Chinese Academy of Sciences, Guiyang 550081, China

**Abstract:** In order to explore the formation age and origin of the tuff within the upper Permian marine limestones at Mapojiao site in the southern Guizhou and its possible relationship with the Emeishan Large Igneous Province (LIP), a study on the bulk rock geochemistry, U-Pb dating, trace elements and Hf isotopic geochemistry of zircon grains of the tuff has been carried out in this paper. The results show that samples of the tuff at Mapojiao display relatively high  $\text{Al}_2\text{O}_3/\text{TiO}_2$  ratios and obvious negative Eu anomalies. The U-Pb ages of zircon grains from two samples are  $(259.1 \pm 1.5)$  Ma and  $(257.5 \pm 1.8)$  Ma, respectively. They are similar to that of the felsic ignimbrite in the Binchuan area. The  $\varepsilon_{\text{Hf}}(t)$  values of zircons from the tuff samples vary from  $+1.1$  to  $+8.4$ , and the Th/Nb ratios of those zircons are relatively low, indicating that they have geochemical characteristics of the intraplate magmatic rocks. The above U-Pb ages and geochemical characteristics of zircons imply that the tuff at Mapojiao could be sourced from the felsic volcanic activity related to the Emeishan LIP. Combined with the published ages of high-precision CA-TIMS zircon U-Pb dating and conodont biostratigraphy, it is believed that the Emeishan felsic volcanism could at least last to the Early Wuchiapingian epoch of the Late Permian. The Emeishan felsic volcanic eruption could be an important factor resulting in the climate cooling in the Wuchiapingian epoch.

**Key words:** tuff; geochemistry; zircon U-Pb age; Hf isotope; Emeishan Large Igneous Province; climate cooling

收稿编号:2021-124, 2021-7-30 收到, 2021-12-7 改回

基金项目:国家自然科学基金资助项目(41972103, 41502109)

第一作者简介:杨晨晨(1997-), 男, 硕士研究生, 古生物学与地层学专业. E-mail: yangchen623@hotmail.com.

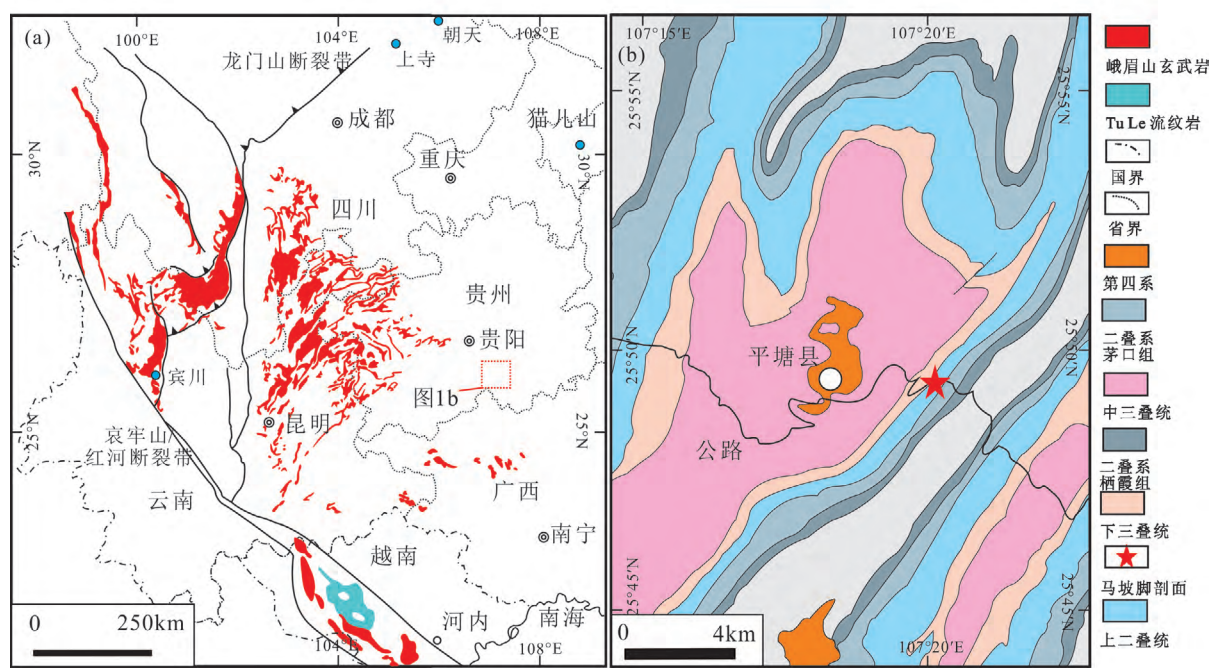
\*通信作者简介:黄虎(1987-), 男, 副教授, 主要从事沉积地球化学研究. E-mail: huanghu118@cdut.edu.cn; 118huanghu@163.com.

## 0 引言

峨眉山大火成岩省主要分布在我国西南地区及越南北部(图1a)(Xu et al., 2001; Ali et al., 2010)。围绕峨眉山大火成岩省的年代学、岩石学、岩浆演化和动力学等已有大量研究工作,但对其精确的火山活动持续时间仍存在较多争议(Shellnutt, 2014; 陈军和徐义刚, 2017)。Sun等(2010)通过对华南多个地层剖面玄武岩夹层或玄武岩下伏灰岩中的牙形石的研究,认为峨眉山玄武岩最早喷发的时间对应中二叠世卡匹敦期的牙形石*J. altudaensis*带,火山活动顶峰对应牙形石*J. xuanhanensis*带。生物地层学、磁性地层学和锆石U-Pb年龄等研究将峨眉山火山活动的主要时间约束在260 Ma左右,即可能结束于中二叠世末期,持续时间约1~2 Ma(He et al., 2007; Sun et al., 2010; Zheng et al., 2010; Zhong et al., 2014; Huang et al., 2016)。然而,越南北部地区的Tu Le流纹岩的锆石CA-TIMS年龄[(259.1±0.6)~(257.9±0.3) Ma]显示峨眉山大火成岩省的火山活动可能持续至晚二叠世吴家坪期(Shellnutt et al., 2020)。

地质历史时期,大火成岩省事件常常与环境剧变与生物灭绝密切相关(Bond et al., 2014; Mather, 2015)。了解大火成岩省精确的火山活

动时限对理解其与生物和环境变化的耦合关系至关重要。华南上二叠统地层中分布有大量的凝灰岩层,这些凝灰岩层有助于研究火山活动影响及精确约束地层年代(Mundil et al., 2004; Shen et al., 2010, 2011)。根据已有研究,在晚二叠世早期全球发生了一次显著的气候变冷事件(Metcalfe et al., 2015),峨眉山大火成岩省的火山活动是否持续到晚二叠世早期,对认识这一气候变冷事件的成因具有重要意义。贵州南部的马坡脚剖面出露上二叠统海相碳酸盐岩夹凝灰岩(Bagherpour et al., 2018a)。该剖面所记录的晚二叠世早期的碳酸盐岩台地沉降、碳同位素漂移及锶同位素比值的降低,都被认为可能与峨眉山大火成岩省的火山活动有关(Bagherpour et al., 2018a, 2018b)。该剖面中的灰岩已有学者开展过详细的牙形石生物地层学研究(Bagherpour et al., 2018a),这为凝灰岩的形成时间提供了生物年代学约束。Fortes De Lena(2019)对这一灰岩夹层中的凝灰岩还开展过高精度年代学研究。但是,目前对这些凝灰岩尚未开展过成因分析,其是否与峨眉山大火成岩省的火山活动有关值得进一步研究。本文对马坡脚剖面上二叠统吴家坪组凝灰岩进行全岩地球化学、锆石U-Pb年龄、锆石微量元素及Hf同位素分析,并对其成



(a) 修改自:Ali等(2010),Xu等(2001);(b)修改自:Bagherpour等(2018a)

图1 峨眉山大火成岩省地质简图(a)及平塘地区地质图(b)

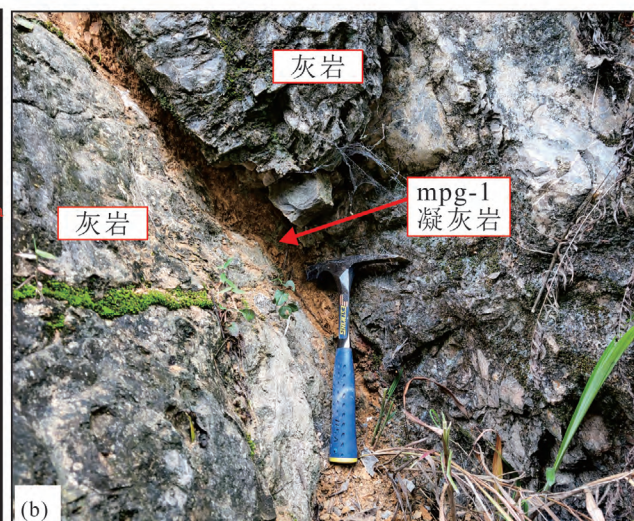
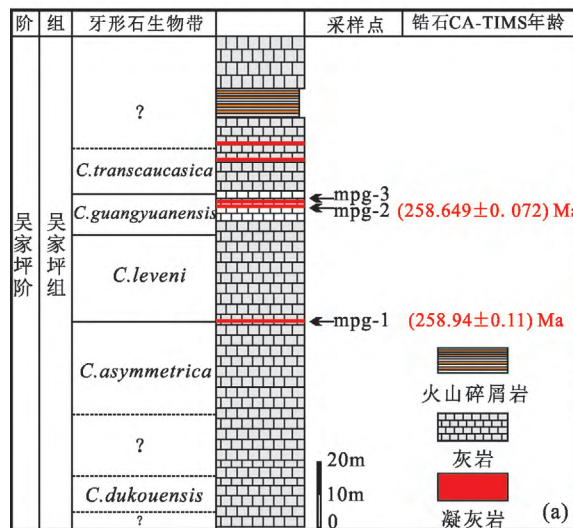
Fig. 1 Geological sketch of the Emeishan Large Igneous Province (a) and geological map of the Pingtang area (b)

因及其与峨眉山大火成岩省火山活动终止时限的潜在关系进行讨论。

## 1 地质背景

峨眉山大火成岩省的出露面积约  $2.5 \times 10^5 \text{ km}^2$  (图 1a), 火山岩厚度变化较大。在大火成岩省西部地区(如云南宾川), 火山岩厚约 5 km, 而在东部贵州厚度仅为数百米(Xu et al., 2001)。峨眉山大火成岩省火山序列主要由大量的玄武岩构成, 包含少量的火山碎屑岩、苦橄岩、粗面岩和流纹岩等(Xu et al., 2001, 2008, 2010; Zhou et al., 2002, 2005, 2006; Shellnutt et al., 2011)。在大火成岩省西部地区, 火山序列主要由底部的低钛玄武岩、上部的高钛玄武岩和顶部的酸性火山岩组成, 而在东部则主要为高钛玄武岩(Xu et al., 2001; Xiao et al., 2004)。

本文研究区域位于贵州省南部平塘地区, 区内发育下二叠统-中三叠统地层(图 1b)。马坡脚剖面位于平塘县以东约 5 km 公路旁。该剖面出露上二叠统吴家坪组, 其岩性主要为灰色-黑色生物碎屑灰岩, 厚约 150 m。剖面上部发育厚约 8 m 的火山碎屑岩, 下部主要为灰岩夹凝灰岩(Bagherpour et al., 2018a)。Bagherpour 等(2018a)对该剖面的牙形石生物地层进行了详细研究, 自下而上共鉴别出 5 个牙形石带。其中, *Clarkina dukouensis* 带出现在最下部, *C. asymmetrica* 带、*C. leveni* 带、*C. guangyuanensis* 带和 *C. transcaucasica* 带出现在剖面中、上部(图 2a)。



牙形石生物带数据引自 Bagherpour 等(2018a); 凝灰岩锆石高精度 CA-TIMS 年龄引自 Fortes De Lena(2019)

图 2 马坡脚剖面地层柱状图(a)及野外照片(b)

Fig. 2 Stratigraphic column (a) and field photograph (b) of the tuff of the Mapojiao section

## 2 样品及测试方法

马坡脚剖面共发育 5 层凝灰岩(Bagherpour et al., 2018a)。因剖面现被植物覆盖, 本次研究在其 3 层获得凝灰岩样品。凝灰岩层在野外呈黄褐色黏土状, 厚度 5~10 cm。采样位置及野外照片见图 2。其中, 样品 mpg-1 位于 *C. leveni* 牙形石生物带底部, 而样品 mpg-2 和 mpg-3 位于 *C. guangyuanensis* 牙形石生物带中上部。因样品蚀变严重, 因此未制作薄片进行镜下观察。3 件样品均进行全岩地球化学分析, 选取样品 mpg-1 和 mpg-2 进行锆石 U-Pb 定年和 Hf 同位素分析。

样品的全岩主量元素含量分析由澳实矿物实验室完成, 采用仪器为 X 射线荧光光谱 XRF。全岩微量元素含量分析由中国地质大学(武汉)地质过程与矿产资源国家重点实验室完成, 采用仪器为 Agilent 7500a ICP-MS。ICP-MS 分析的样品处理过程包括:①称取粉碎至大约 200 目的岩石粉末 50 mg 于 Teflon 溶样器中; ②采用 Teflon 溶样弹将样品用 HF+HNO<sub>3</sub> 在 195 °C 条件下消解 48 h; ③将在 120 °C 条件下蒸干除 Si 后的样品用 2% HNO<sub>3</sub> 稀释 2000 倍, 定容于干净的聚酯瓶。详细的样品消解处理过程、分析精密度和准确度见 Liu 等(2008b)。

分析锆石由河北省廊坊地质研究院采用常规重液和电磁进行分选, 分选出的锆石在武汉上谱分析科技有限责任公司制样。用环氧树脂将锆石制靶后磨蚀抛光至锆石平面暴露约 1/3~1/2, 经阴极发光图像分析锆石颗粒的内部结构并选取最佳测

试点位置。锆石 U-Pb 定年和微量元素分析在武汉上谱分析科技有限责任公司用 LA-ICP-MS 仪分析。激光剥蚀系统为 GeoLas 2005, ICP-MS 为 Agilent 7500a。激光剥蚀过程中采用氦气作载气、氩气为补偿气,二者在进入 ICP 之前通过一个 T 型接头混合。在等离子体中心气流 (Ar+He) 中加入少量氮气,以提高仪器灵敏度、降低检出限和改善分析精密度 (Hu et al., 2008)。另外,激光剥蚀系统配置一个信号平滑装置,即使激光脉冲频率低达 1 Hz,采用该装置后也能获得光滑的分析信号 (Hu et al., 2012b)。每个时间分辨分析数据包括大约 20~30 s 的空白信号和 50 s 的样品信号。对分析数据采用软件 ICPMSDataCal (Liu et al., 2008a, 2010a) 进行处理。详细的仪器操作条件和数据处理方法见 Liu 等 (2008a, 2010a, 2010b)。

锆石微量元素含量利用多个 USGS 参考玻璃 (BCR-2G, BIR-1G) 为多外标、Si 作内标的方法进行定量计算 (Liu et al., 2010a)。USGS 玻璃中元素含量的推荐值据 GeoReM 数据库 (<http://georem.mpcg-mainz.gwdg.de/>)。U-Pb 同位素定年中采用标准锆石 91500 作外标,每分析 5 个样品点,分析 2 次 91500。对于与分析时间有关的 U-Th-Pb 同位素比值漂移,利用 91500 的变化采用线性内插方式进行校正 (Liu et al., 2010a)。锆石标准 91500 的 U-Th-Pb 同位素比值推荐值据 Wiedenbeck 等 (1995)。锆石样品的 U-Pb 年龄谐和图绘制和年龄权重计算均采用 Isoplot 软件完成 (Ludwig, 2003)。

锆石 Hf 同位素分析在中国地质大学(武汉)地质过程与矿产资源国家重点实验室完成,分析仪器为 GeoLas 2005 ARF 准分子激光剥蚀系统及德国赛默飞世尔科技公司生产的 MC-ICP-MS。激光剥蚀系统、MC-ICP-MS 测试条件与同位素分馏校正见文献 (Liu, 2010b; Hu et al., 2012a)。 $\varepsilon_{\text{Hf}}(t)$  值计算采用的  $^{176}\text{Lu}$  衰变常数为  $1.867 \times 10^{-11}$  (Scherer et al., 2001), 现今球粒陨石  $^{176}\text{Lu}/^{177}\text{Hf}$  值为 0.033,  $^{176}\text{Hf}/^{177}\text{Hf}$  值为 0.283 (Blichert-Toft and Albarède, 1997);一阶段 Hf 模式年龄  $t_{\text{DM1}}$  计算采用的现今亏损地幔  $^{176}\text{Lu}/^{177}\text{Hf}$  值为 0.038,  $^{176}\text{Hf}/^{177}\text{Hf}$  值为 0.283 (Griffin et al., 2000);二阶段 Hf 模式年龄  $t_{\text{DM2}}$  计算采用的亏损地幔  $f_{\text{DM}}$  值为 0.015 (Griffin et al., 2000)。

### 3 分析结果

#### 3.1 全岩主、微量元素

样品全岩主量元素分析结果(表 1)显示,马

表 1 马坡脚剖面凝灰岩样品的全岩主量和微量元素分析结果

Table 1 Analytical results of major and trace elements of bulk rocks of the samples of the tuff of the Mapojiao section

样品编号	mpg-1	mpg-2	mpg-3
SiO <sub>2</sub>	49.07	57.20	55.46
TiO <sub>2</sub>	1.02	0.79	0.74
Al <sub>2</sub> O <sub>3</sub>	23.21	19.88	19.34
TFe <sub>2</sub> O <sub>3</sub>	8.49	2.18	6.55
MnO	0.05	<0.01	0.02
MgO	2.93	4.47	4.22
CaO	0.86	0.85	0.44
Na <sub>2</sub> O	0.04	0.03	0.03
K <sub>2</sub> O	5.74	5.96	5.14
P <sub>2</sub> O <sub>5</sub>	0.12	0.04	0.07
烧失量	7.54	6.97	7.37
CIA	79	75	77
Sc	4.78	6.11	5.06
V	44.20	4.00	4.20
Cr	8.17	1.35	1.94
Ni	61.3	1.3	8.1
Cu	14.6	3.0	5.5
Zn	429	120	305
Rb	125	132	119
Sr	62.1	45.6	34.6
Y	99.8	183	106
Zr	2464	3196	1438
Nb	226	439	235
Ba	66.5	28.2	25.8
La	282	185	175
Ce	604	437	361
Pr	79.7	50.0	41.2
Nd	294	177	145
Sm	50.3	38.6	25.7
Eu	5.96	3.08	2.67
Gd	38.1	34.8	20.1
Tb	5.39	6.05	3.47
Dy	27.4	35.9	21.0
Ho	4.37	7.23	4.11
Er	10.4	20.9	11.0
Tm	1.29	3.46	1.61
Yb	7.42	23.3	10.2
Lu	1.00	3.59	1.45
Hf	59.5	76.2	34.0
Ta	19.2	27.7	13.4
Th	54.1	53.0	33.3
U	5.61	16.4	8.33
Eu/Eu <sup>*</sup>	0.42	0.26	0.36

注: 主量元素(%) 和微量元素( $\times 10^{-6}$ ) 含量均为质量分数; CIA =  $[\text{Al}_2\text{O}_3 / (\text{Al}_2\text{O}_3 + \text{CaO}^* + \text{Na}_2\text{O} + \text{K}_2\text{O})] \times 100$  (Nesbitt and Young, 1982), 其中, 氧化物所用含量为摩尔含量, CaO<sup>\*</sup> 是根据 McLenan 等 (1993) 提出的方法校正的硅酸盐中的 CaO; Eu/Eu<sup>\*</sup> =  $2\text{Eu}_{\text{N}} / (\text{Sm}_{\text{N}} + \text{Gd}_{\text{N}})$ , 下标“N”表示为球粒陨石标准化值。

坡脚凝灰岩样品的烧失量较高(6.97%~7.54%)。3个样品的 $\text{SiO}_2$ 含量为49.07%~57.20%, $\text{Al}_2\text{O}_3$ (平均20.81%)和 $\text{TiO}_2$ 含量(平均0.85%)较高, $\text{Al}_2\text{O}_3/\text{TiO}_2$ 比值分别为22.8、25.2和26.1,计算得到的化学蚀变指数(CIA)分别为79、75和77。

在球粒陨石标准化稀土元素配分模式图中,3个样品的配分模式相似,均表现为轻稀土富集、重稀土亏损,且有明显的Eu负异常(图3a)( $\text{Eu}/\text{Eu}^*$ 值分别为0.42、0.26和0.36)。在原始地幔标准化蛛网图中,3个样品均具显著的Ba、Sr和Ti负异常。其中,样品mpg-1显示Nb负异常,其余样品均缺失Nb、Ta负异常(图3b)。

### 3.2 锆石U-Pb年龄

本次用于分析的2个样品(mp-1和mpg-2)中的锆石呈无色或浅黄色,多为半自形-自形柱状, $\text{Th}/\text{U}$ 比值为0.48~1.46,平均0.71(表2),阴极发光图像显示清晰的震荡环带(图4),应为典型的岩

浆锆石(Hoskin and Schaltegger, 2003)。

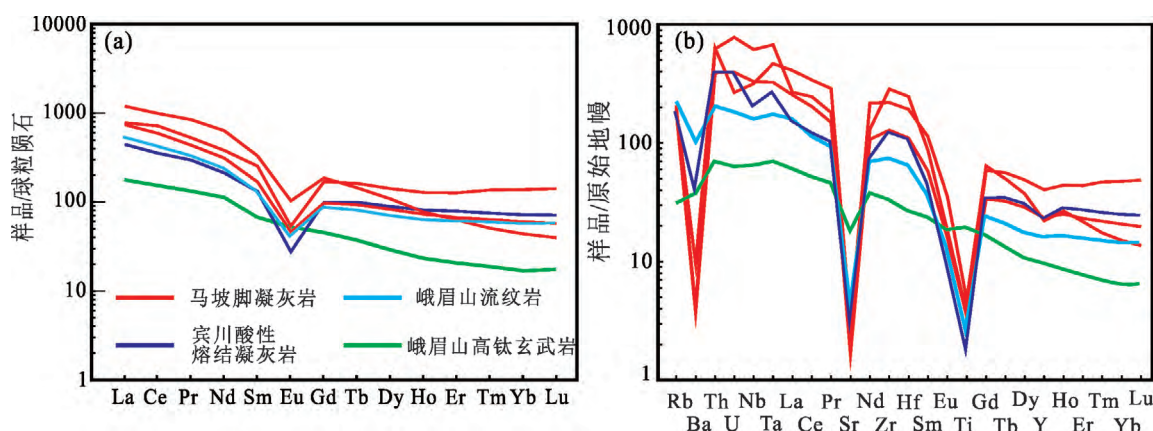
样品mpg-1中的29个锆石分析点中的21个点的谐和度大于90%,年龄为265~255 Ma,加权平均年龄为( $259.1 \pm 1.5$ ) Ma(MSWD=0.33)(图5a)。样品mpg-2的30个分析点中的18个点的谐和度大于90%,年龄为262~255 Ma,加权平均年龄为( $257.5 \pm 1.8$ ) Ma(MSWD=0.20)(图5b)。

### 3.3 锆石微量、稀土元素

mpg-1和mpg-2样品中锆石的微量、稀土元素分析结果见表3。在球粒陨石标准化稀土元素配分模式图中,所有分析的锆石都具有相似的微量元素组成,均表现为轻稀土亏损、重稀土异常富集,总体呈现出由La向Lu急剧增加的趋势,且具有明显的Ce正异常及Eu负异常特征(图6)。

### 3.4 锆石Hf同位素

对mpg-1和mpg-2样品中的25颗年龄为260 Ma左右的锆石进行原位微区Lu-Hf同位素分析

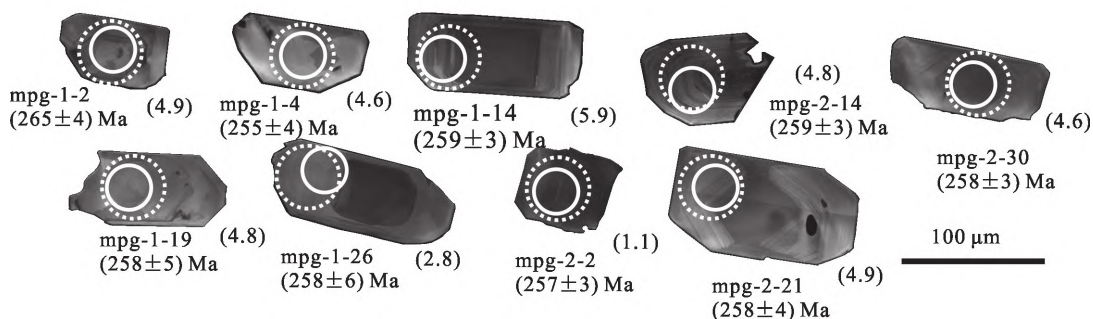


峨眉山玄武岩数据引自Xiao等(2004)和Xu等(2001);峨眉山流纹岩数据引自Xu等(2010);宾川酸性熔结凝灰岩

数据引自Huang等(2018);球粒陨石及原始地幔标准化值引自Sun和McDonough(1989)

图3 马坡脚剖面凝灰岩样品的球粒陨石标准化稀土元素配分模式图(a)和原始地幔标准化蛛网图(b)

Fig. 3 Chondrite-normalized REE patterns (a) and Primitive mantle-normalized trace elements spider diagrams (b) of the samples of the tuff of the Mapojiao section



虚线圆圈为U-Pb分析点,实线圆圈为Hf分析点,括号内数据为 $\epsilon\text{Hf}(t)$ 值

图4 马坡脚凝灰岩代表性锆石阴极发光图像

Fig. 4 CL images of representative zircons from the tuff at Mapojiao

表2 锆石U-Pb同位素分析结果  
Table 2 Analytical results of U-Pb isotopes of zircon grains

点号	元素含量/( $\times 10^{-6}$ )		同位素比值				年龄/Ma				谐和度							
	Pb	Th	U	Th/U	$^{207}\text{Pb}/^{206}\text{Pb}$	$1\sigma$	$^{207}\text{Pb}/^{235}\text{U}$	$1\sigma$	$^{206}\text{Pb}/^{238}\text{U}$	$1\sigma$		$^{207}\text{Pb}/^{206}\text{Pb}$	$1\sigma$	$^{207}\text{Pb}/^{235}\text{U}$	$1\sigma$	$^{206}\text{Pb}/^{238}\text{U}$	$1\sigma$	
mpg-1-01	10	55	83	0.66	0.0524	0.0037	0.2900	0.0178	0.0415	0.0007	0.2767	302	161	259	14	262	4	98%
mpg-1-02	17	93	126	0.73	0.0526	0.0030	0.3043	0.0165	0.0420	0.0006	0.2598	322	131	270	13	265	4	98%
mpg-1-03	7	38	68	0.56	0.0612	0.0058	0.3321	0.0282	0.0403	0.0008	0.2325	656	206	291	22	255	5	86%
mpg-1-04	11	64	91	0.71	0.0513	0.0038	0.2810	0.0168	0.0403	0.0007	0.2770	254	168	251	13	255	4	98%
mpg-1-05	17	86	85	1.00	0.1203	0.0064	0.6907	0.0383	0.0417	0.0008	0.3293	1961	94	533	23	264	5	32%
mpg-1-06	23	72	97	0.74	0.1239	0.0057	0.8299	0.0380	0.0487	0.0008	0.3376	2013	83	614	21	307	5	33%
mpg-1-07	13	75	105	0.72	0.0597	0.0044	0.3212	0.0214	0.0399	0.0006	0.2419	591	155	283	16	252	4	88%
mpg-1-08	9	52	79	0.66	0.0578	0.0049	0.3151	0.0239	0.0404	0.0007	0.2226	524	185	278	18	255	4	91%
mpg-1-09	17	99	131	0.76	0.0521	0.0032	0.2946	0.0167	0.0410	0.0006	0.2538	300	143	262	13	259	4	98%
mpg-1-10	12	73	97	0.75	0.0661	0.0045	0.3555	0.0224	0.0394	0.0007	0.2857	809	143	309	17	249	4	78%
mpg-1-11	9	56	79	0.71	0.0631	0.0049	0.3497	0.0252	0.0412	0.0007	0.2347	722	135	305	19	260	4	84%
mpg-1-12	8	44	70	0.63	0.0547	0.0045	0.3070	0.0240	0.0411	0.0008	0.2557	398	183	272	19	260	5	95%
mpg-1-13	12	72	100	0.72	0.0564	0.0041	0.3170	0.0210	0.0406	0.0006	0.2361	478	166	280	16	257	4	91%
mpg-1-14	28	162	222	0.73	0.0510	0.0027	0.2878	0.0148	0.0410	0.0004	0.2106	239	122	257	12	259	3	99%
mpg-1-15	7	39	65	0.60	0.0573	0.0048	0.3156	0.0236	0.0407	0.0007	0.2302	502	187	279	18	257	4	92%
mpg-1-16	19	113	176	0.64	0.0574	0.0035	0.3228	0.0187	0.0409	0.0005	0.2081	506	135	284	14	258	3	90%
mpg-1-17	11	50	81	0.61	0.0741	0.0051	0.4379	0.0293	0.0431	0.0008	0.2932	1056	138	369	21	272	5	69%
mpg-1-18	11	60	100	0.60	0.0542	0.0034	0.3039	0.0177	0.0412	0.0006	0.2581	389	145	269	14	261	4	96%
mpg-1-19	8	48	70	0.69	0.0515	0.0045	0.2783	0.0211	0.0408	0.0008	0.2438	261	197	249	17	258	5	96%
mpg-1-20	88	553	548	1.01	0.0523	0.0018	0.2954	0.0098	0.0408	0.0004	0.3004	298	78	263	8	258	3	98%
mpg-1-21	6	31	58	0.53	0.0549	0.0047	0.2993	0.0218	0.0409	0.0008	0.2782	409	190	266	17	259	5	97%
mpg-1-22	13	76	113	0.67	0.0526	0.0033	0.2950	0.0183	0.0411	0.0007	0.2598	322	144	262	14	259	4	98%
mpg-1-23	33	182	258	0.71	0.0533	0.0024	0.3014	0.0132	0.0412	0.0005	0.2870	343	100	267	10	260	3	97%
mpg-1-24	76	483	493	0.98	0.0493	0.0017	0.2802	0.0095	0.0411	0.0003	0.2484	161	80	251	8	260	2	96%
mpg-1-26	7	37	66	0.56	0.0555	0.0051	0.2924	0.0224	0.0409	0.0009	0.2970	432	210	260	18	258	6	99%
mpg-1-27	34	220	223	0.99	0.0515	0.0028	0.2880	0.0150	0.0408	0.0005	0.2410	261	94	257	12	258	3	99%
mpg-1-28	9	49	82	0.60	0.0551	0.0041	0.3124	0.0226	0.0412	0.0007	0.2434	417	169	276	17	260	4	94%
mpg-1-29	31	192	220	0.87	0.0524	0.0026	0.2975	0.0149	0.0412	0.0005	0.2547	302	113	264	12	260	3	98%
mpg-1-30	11	59	74	0.80	0.0717	0.0055	0.3843	0.0258	0.0403	0.0007	0.2756	977	157	330	19	254	5	74%

续表2

点号	元素含量/( $\times 10^{-6}$ )		同位素比值						年龄/Ma									
	Pb	Th	$^{207}\text{Pb}/^{206}\text{Pb}$	$1\sigma$	$^{207}\text{Pb}/^{235}\text{U}$	$1\sigma$	$^{206}\text{Pb}/^{238}\text{U}$	$1\sigma$	$\text{rho}$	$^{207}\text{Pb}/^{206}\text{Pb}$	$1\sigma$	$^{207}\text{Pb}/^{235}\text{U}$	$1\sigma$	$^{206}\text{Pb}/^{238}\text{U}$	$1\sigma$	谐和度		
mpg-2-01	40	241	334	0.72	0.0518	0.0021	0.2889	0.0120	0.0403	0.0004	0.2648	280	90	258	9	255	3	98%
mpg-2-02	55	331	463	0.72	0.0515	0.0017	0.2877	0.0091	0.0406	0.0004	0.3130	261	81	257	7	257	3	99%
mpg-2-03	11	53	91	0.58	0.0695	0.0049	0.3897	0.0238	0.0415	0.0008	0.3052	922	146	334	17	262	5	75%
mpg-2-04	10	59	98	0.61	0.0601	0.0049	0.3315	0.0234	0.0408	0.0007	0.2519	609	178	291	18	258	4	87%
mpg-2-05	11	63	96	0.66	0.0532	0.0045	0.2892	0.0225	0.0408	0.0008	0.2666	345	193	258	18	258	5	99%
mpg-2-06	13	56	95	0.59	0.0765	0.0052	0.4434	0.0281	0.0421	0.0007	0.2501	1107	136	373	20	266	4	66%
mpg-2-07	18	77	160	0.48	0.0742	0.0053	0.4282	0.0345	0.0407	0.0007	0.1991	1047	143	362	25	257	4	66%
mpg-2-08	15	81	152	0.54	0.0555	0.0060	0.2861	0.0189	0.0403	0.0009	0.3403	432	244	256	15	255	6	99%
mpg-2-09	117	815	558	1.46	0.0573	0.0043	0.3086	0.0152	0.0407	0.0011	0.5704	506	167	273	12	257	7	94%
mpg-2-10	10	54	86	0.63	0.0497	0.0045	0.2688	0.0220	0.0404	0.0007	0.2031	189	200	242	18	256	4	94%
mpg-2-11	37	250	329	0.76	0.0486	0.0022	0.2793	0.0146	0.0414	0.0011	0.5046	132	109	250	12	262	7	95%
mpg-2-12	19	111	149	0.75	0.0586	0.0038	0.3305	0.0227	0.0405	0.0006	0.2080	554	147	290	17	256	4	87%
mpg-2-13	50	267	274	0.97	0.0852	0.0040	0.4880	0.0240	0.0411	0.0006	0.2935	1320	91	404	16	260	4	56%
mpg-2-14	30	171	249	0.68	0.0534	0.0024	0.3009	0.0133	0.0409	0.0005	0.2891	343	102	267	10	259	3	96%
mpg-2-15	37	161	273	0.59	0.0750	0.0027	0.4311	0.0146	0.0417	0.0005	0.3291	1069	72	364	10	264	3	68%
mpg-2-16	17	99	168	0.59	0.0513	0.0023	0.2836	0.0123	0.0405	0.0005	0.3094	254	110	254	10	256	3	99%
mpg-2-17	12	63	96	0.66	0.0654	0.0042	0.3666	0.0226	0.0409	0.0006	0.2449	787	137	317	17	259	4	79%
mpg-2-18	19	105	185	0.57	0.0530	0.0035	0.2981	0.0147	0.0410	0.0005	0.2469	332	117	265	11	259	3	97%
mpg-2-19	11	66	102	0.65	0.0516	0.0032	0.2899	0.0165	0.0409	0.0006	0.2793	333	175	258	13	259	4	99%
mpg-2-20	15	80	125	0.64	0.0554	0.0032	0.3089	0.0172	0.0410	0.0007	0.2909	432	130	273	13	259	4	94%
mpg-2-21	13	76	119	0.64	0.0532	0.0035	0.2987	0.0185	0.0409	0.0007	0.2590	345	147	265	15	258	4	97%
mpg-2-22	34	229	213	1.08	0.0690	0.0156	0.3125	0.0354	0.0409	0.0007	0.1608	900	478	276	27	258	5	93%
mpg-2-23	38	248	273	0.91	0.0535	0.0108	0.2602	0.0300	0.0408	0.0033	0.6925	350	400	230	24	258	20	89%
mpg-2-24	27	84	121	0.69	0.1317	0.0080	0.8222	0.0538	0.0440	0.0009	0.3064	2121	107	609	30	278	5	25%
mpg-2-25	20	97	150	0.65	0.0680	0.0040	0.3847	0.0238	0.0407	0.0005	0.2160	878	122	330	17	257	3	75%
mpg-2-26	10	58	97	0.60	0.0470	0.0031	0.2627	0.0158	0.0409	0.0007	0.2792	56	143	237	13	259	4	91%
mpg-2-27	35	194	265	0.73	0.0692	0.0077	0.4021	0.0537	0.0405	0.0006	0.1162	906	230	343	39	256	4	70%
mpg-2-28	12	67	114	0.59	0.0542	0.0033	0.3032	0.0174	0.0411	0.0006	0.2626	389	137	269	14	260	4	96%
mpg-2-29	6	33	50	0.67	0.0575	0.0052	0.3103	0.0240	0.0408	0.0009	0.2886	522	198	274	19	258	6	93%
mpg-2-30	15	90	123	0.73	0.0500	0.0030	0.2816	0.0163	0.0408	0.0005	0.2090	195	136	252	13	258	3	97%

表3 马坡脚凝灰岩锆石微量元素分析结果

Table 3 Analytical results of trace elements and REE of zircon grains from the tuff at Mapoqiao

点号	Ti	Y	Nb	La	Ce	Pr	Nd	Sm	Eu	Gd	Tb	Dy	Ho	Er	Tm	Yb	Lu	Hf	Ta	Th	U
mpg-1-04	12.8	1388	5.58	0.16	12.3	1.11	9.22	12.5	1.53	46.2	14.6	1.57	53.2	208	42.0	366	57.4	8165	2.22	65.8	90.9
mpg-1-07	263	1473	21.4	0.31	15.7	1.67	11.6	15.0	1.86	50.1	15.5	1.69	56.8	223	44.5	381	60.1	7728	3.14	77.6	105
mpg-1-08	20.9	1253	6.67	0.21	11.8	1.15	8.48	11.9	1.17	41.9	13.0	1.40	47.9	190	38.4	327	52.4	8225	2.13	55.5	80.8
mpg-1-11	15.8	987	4.14	0.040	9.33	0.50	4.38	7.02	0.98	28.6	9.42	1.09	37.2	152	31.5	277	45.0	8716	1.69	56.6	77.7
mpg-1-12	14.9	996	4.49	0.042	7.02	0.59	4.58	6.74	1.11	29.8	9.8	1.12	37.9	149	31.3	281	43.8	8496	1.95	46.2	70.6
mpg-1-13	16.8	1219	5.67	0.18	10.6	0.70	5.95	8.92	1.07	37.4	12.0	1.36	47.0	189	38.6	337	54.0	9255	2.12	75.1	103
mpg-1-14	10.00	1555	14.3	0.087	24.1	0.83	6.85	11.0	0.66	46.9	14.9	1.75	60.2	235	47.7	392	60.1	8576	4.19	162	219
mpg-1-16	10.1	1917	6.31	0.072	11.2	1.52	12.1	15.7	1.13	67.2	20.4	221	74.1	283	57.0	466	71.7	8181	2.40	111	169
mpg-1-18	14.9	1136	6.67	0.08	11.0	0.79	5.42	8.27	0.85	32.9	10.71	1.26	42.6	171	35.8	312	49.5	8578	2.71	63.5	101.1
mpg-1-19	15.0	902	3.74	0.029	8.42	0.39	4.06	6.49	0.85	25.1	8.64	99.7	33.3	140	29.1	254	42.4	8848	1.45	49.0	69.1
mpg-1-21	11.4	614	5.39	0.0050	10.3	0.106	1.49	3.24	0.47	15.1	4.95	64.6	22.6	95.4	20.4	183	30.3	8542	1.73	31.6	58.1
mpg-1-22	9.10	1429	7.95	0.064	14.7	0.91	7.23	11.6	1.42	42.3	14.4	160	54.3	217	43.7	365	59.6	7867	2.88	75.3	110
mpg-1-26	9.36	659	6.11	0.0128	12.0	0.20	1.64	3.83	0.54	16.6	5.84	67.9	24.3	104	21.7	195	30.5	7902	1.93	37.0	65.2
mpg-1-27	13.8	2468	17.5	0.21	33.4	1.48	11.5	19.0	2.19	76.6	24.7	278	94.0	373	74.4	617	95.1	7504	4.70	223	224
mpg-1-28	14.2	810	4.92	0.010	8.74	0.21	2.48	4.99	0.64	21.2	7.13	86.0	30.2	123	26.4	239	38.9	8596	1.86	50.8	81.3
mpg-1-29	7.17	2488	14.3	0.14	28.9	1.53	13.2	17.8	1.93	78.2	24.6	277	95.3	370	74.8	613	96.3	7642	4.30	181	210
mpg-2-02	3.32	2323	44.1	0.021	52.8	0.52	4.47	9.5	0.58	53.3	19.9	246	88.1	359	73.6	605	89.4	7747	10.5	342	463
mpg-2-04	8.19	1214	9.6	0.037	24.0	0.99	6.71	9.8	0.95	36.9	11.7	135	45.0	185	38.6	333	54.8	7156	3.21	59.4	95
mpg-2-06	23.1	922	17.0	0.36	27.9	1.35	3.84	6.11	0.44	23.7	8.22	96.2	34.2	142	30.7	274	45.0	7350	3.31	62.1	99.1
mpg-2-07	8.70	1264	20.5	0.086	23.4	0.62	4.05	7.75	0.43	31.5	10.8	131	46.9	195	41.5	365	58.5	7798	4.85	83.8	164
mpg-2-08	5.36	1871	12.58	0.034	21.2	1.00	7.16	12.2	1.10	48.4	17.5	205	71.0	287	59.8	501	78.8	6873	3.19	84.3	152
mpg-2-10	25.0	1020	19.4	0.24	23.9	1.52	7.9	9.2	0.64	29.6	9.3	106	38.2	153	32.9	290	48.1	6908	2.98	55.8	85.8
mpg-2-16	5.64	1294	16.6	0.014	23.6	0.34	3.28	7.06	0.43	31.5	10.6	130	46.2	199	40.8	346	53.9	7550	3.97	102	167
mpg-2-18	7.44	1246	18.1	0.01	24.1	0.37	2.72	5.95	0.35	28.3	10.0	124	45.0	191	40.1	345	54.5	7700	4.54	106.1	183
mpg-2-19	10.2	1010	11.9	0.031	29.4	0.41	3.24	6.05	0.55	23.6	8.47	103	35.4	152	33.3	296	48.1	7336	3.25	69.7	103
mpg-2-22	11.4	2545	16.0	0.15	29.4	1.50	15.2	22.0	1.08	78.5	25.1	274	93	367	75.6	635	103	6677	3.63	242	219
mpg-2-26	7.82	945	11.1	0.062	23.8	0.40	3.42	6.83	0.49	23.9	7.99	94.2	33.4	140	30.6	264	44.1	6954	2.95	59.9	96.5

注:微量元素和稀土元素含量均为质量分数( $\times 10^{-6}$ )。

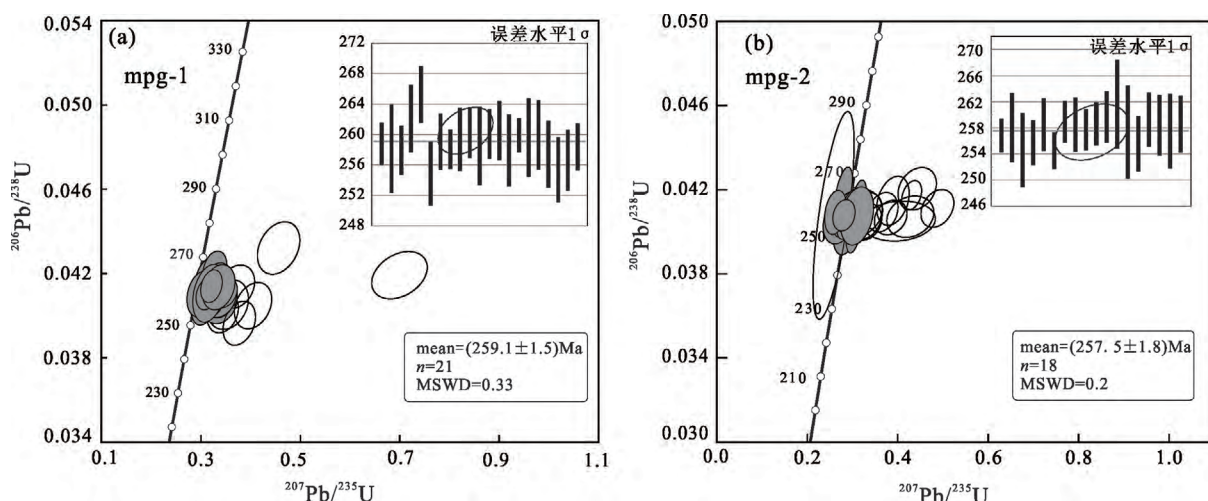
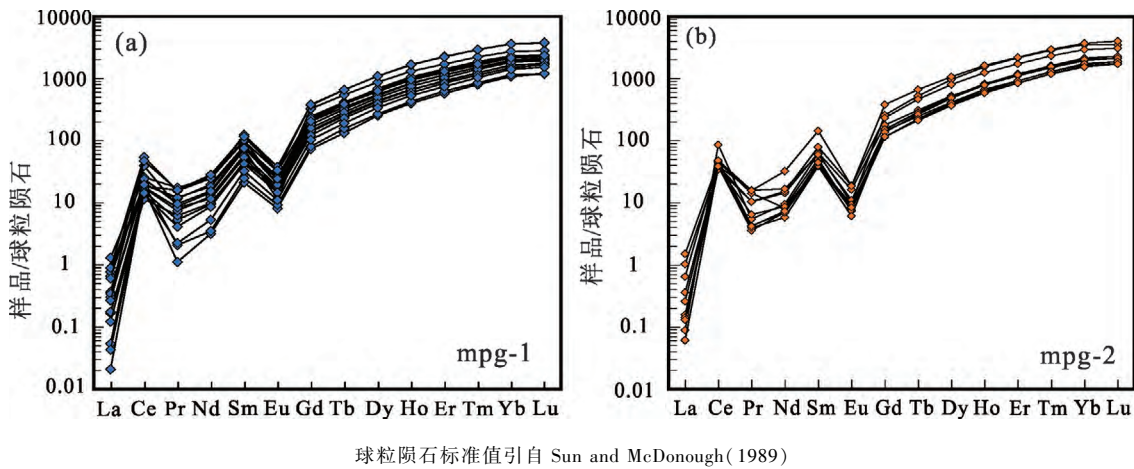


图 5 马坡脚凝灰岩锆石 U-Pb 年龄谐和图

Fig. 5 Concordia diagrams of zircon U-Pb ages from the tuff at Mapojiao



球粒陨石标准值引自 Sun and McDonough (1989)

图 6 马坡脚凝灰岩中锆石球粒陨石标准化稀土元素配分模式图

Fig. 6 Chondrite-normalized REE patterns of zircons from the tuff at Mapojiao

(表 4),结果显示 2 个样品的锆石  $\epsilon_{\text{hf}}(t)$  均为正值,为 1.1~8.4,平均 4.7。

## 4 讨论

### 4.1 马坡脚剖面凝灰岩的成因

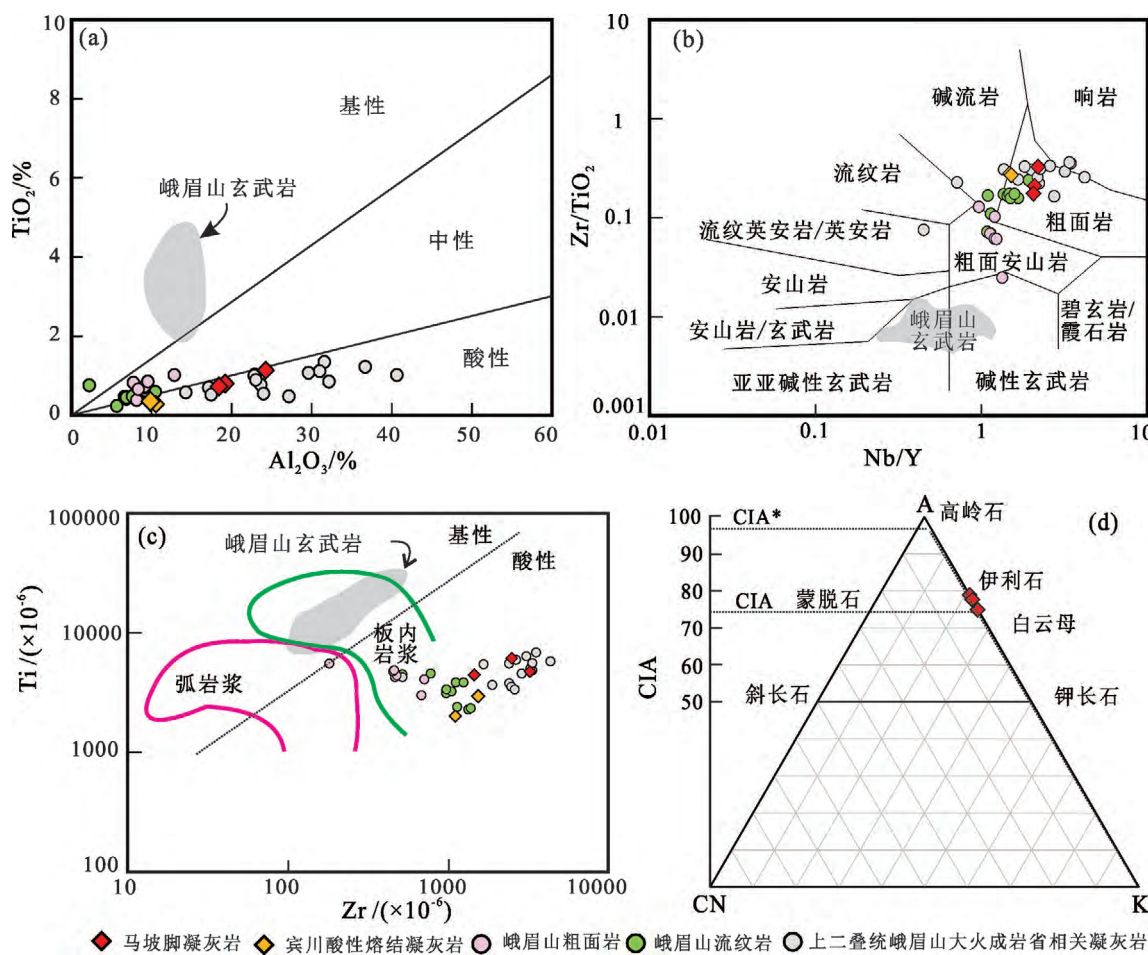
未风化的岩浆岩的 CIA 值通常为 30~55,而纯铝硅酸盐风化的最终产物(如高岭石)则接近 100 (Nesbitt and Young, 1982)。钾交代作用会造成 CIA 计算值偏低,使用 A-CN-K 三角图(图 7d)可以校正样品钾交代之前的 CIA 值(Nesbitt and Young, 1989; Fedo et al., 1995)。马坡脚凝灰岩样品经校正后的 CIA 值大于 95(图 7d),证实其遭受了强烈的风化蚀变作用。 $\text{Al}_2\text{O}_3/\text{TiO}_2$  比值及稳定的高场强元素(如 Nb、Ti、Zr、Ta、Hf、Sc 和 Th 等)不易受风化影响,常用来解释岩浆来源(Winchester and Floyd, 1977; Hayashi et al., 1997)。其中,基性岩浆

$\text{Al}_2\text{O}_3/\text{TiO}_2$  的比值为 3~8,中性岩浆为 8~21,而酸性岩浆为 21~70(Hayashi et al., 1997)。马坡脚凝灰岩 3 个样品的  $\text{Al}_2\text{O}_3/\text{TiO}_2$  比值分别为 22.8、25.2 和 26.1,较基性和中性岩浆岩的高(图 7a)。在  $\text{Nb}/\text{Y-Zr}/\text{TiO}_2$  判别图中(图 7b),样品点均落入粗面岩区域,与宾川熔结凝灰岩和峨眉山流纹岩接近。 $\text{Zr}/\text{Ti}$  之间的相关性可作为判断岩浆活动构造环境和火成岩类的依据(Pearce, 1982)。在  $\text{Zr-Ti}$  判别图中(图 7c),马坡脚凝灰岩样品点落在酸性岩浆范围,且靠近板内熔岩区域。总体上看,马坡脚凝灰岩的主、微量元素特征与宾川熔结凝灰岩、峨眉山流纹岩等酸性火山岩相似(图 7)。因此,我们认为马坡脚剖面凝灰岩可能是酸性火山活动的产物。

在晚二叠世,锆石年龄为 260~252 Ma 的大陆岩浆弧活动在华南板块周缘异常活跃(Li et al., 2006; Zhu et al., 2009; Zi et al., 2013; Hu et al.,

表 4 锯石 Hf 同位素分析结果  
Table 4 Analytical results of Hf isotope of zircon grains

样 号	$^{176}\text{Hf}/^{177}\text{Hf}$	$1\sigma$	$^{176}\text{Lu}/^{177}\text{Hf}$	$1\sigma$	$^{176}\text{Yb}/^{177}\text{Hf}$	$1\sigma$	$t/\text{Ma}$	$\varepsilon_{\text{Hf}}(t)$	$1\sigma$	$t_{\text{DM}}$	$t_{\text{DW}}$	$f_{\text{Lu/Hf}}$	
mpg-1-02	0.282753	0.000048	0.0017	0.000013	0.0623	0.000560	265	-0.7	4.9	1.8	719	887	-0.95
mpg-1-04	0.282750	0.000028	0.0011	0.000002	0.0412	0.000103	255	-0.8	4.6	1.1	713	892	-0.97
mpg-1-09	0.282749	0.000030	0.0012	0.000007	0.0464	0.000417	259	-0.8	4.7	1.2	716	893	-0.96
mpg-1-13	0.282774	0.000031	0.0009	0.000016	0.0347	0.000509	257	0.1	5.6	1.2	676	843	-0.97
mpg-1-14	0.282784	0.000030	0.0012	0.000025	0.0494	0.001211	259	0.4	5.9	1.2	668	825	-0.96
mpg-1-19	0.282750	0.000023	0.0006	0.000001	0.0217	0.000069	258	-0.8	4.8	1.0	704	886	-0.98
mpg-1-20	0.282864	0.000041	0.0032	0.000018	0.1288	0.000529	258	3.3	8.4	1.6	584	686	-0.90
mpg-1-22	0.282762	0.000023	0.0011	0.000004	0.0412	0.000266	259	-0.4	5.1	1.0	697	868	-0.97
mpg-1-23	0.282789	0.000028	0.0022	0.000015	0.0852	0.000354	260	0.6	6.0	1.1	677	823	-0.94
mpg-1-25	0.282801	0.000024	0.0026	0.000072	0.1052	0.003350	260	1.0	6.3	1.3	667	804	-0.92
mpg-1-26	0.282694	0.000041	0.0006	0.000007	0.0210	0.000177	258	-2.7	2.8	1.6	781	996	-0.98
mpg-1-27	0.282723	0.000036	0.0014	0.000007	0.0515	0.000164	258	-1.7	3.7	1.4	757	947	-0.96
mpg-1-28	0.282709	0.000031	0.0007	0.000005	0.0273	0.000316	260	-2.2	3.4	1.2	763	967	-0.98
mpg-1-29	0.282761	0.000028	0.0013	0.000014	0.0481	0.000767	260	-0.4	5.1	1.1	700	870	-0.96
mpg-2-02	0.282654	0.000045	0.0022	0.000016	0.0798	0.000426	257	-4.2	1.1	1.7	875	1092	-0.93
mpg-2-07	0.282707	0.000044	0.0017	0.000034	0.0549	0.000982	257	-2.3	3.1	1.7	787	983	-0.95
mpg-2-14	0.282754	0.000027	0.0015	0.000008	0.0564	0.000461	259	-0.6	4.8	1.1	716	888	-0.95
mpg-2-16	0.282770	0.000030	0.0012	0.000021	0.0441	0.000654	256	-0.1	5.3	1.2	687	854	-0.96
mpg-2-19	0.282787	0.000027	0.0010	0.000003	0.0320	0.000191	259	0.5	6.1	1.1	658	817	-0.97
mpg-2-20	0.282736	0.000027	0.0010	0.000001	0.0355	0.000086	259	-1.3	4.2	1.1	731	918	-0.97
mpg-2-21	0.282757	0.000029	0.0013	0.000003	0.0446	0.000173	258	-0.5	4.9	1.2	708	880	-0.96
mpg-2-23	0.282728	0.000027	0.0012	0.000015	0.0445	0.000608	258	-1.6	3.9	1.1	747	936	-0.96
mpg-2-26	0.282711	0.000030	0.0009	0.000001	0.0322	0.000080	259	-2.2	3.4	1.2	765	967	-0.97
mpg-2-29	0.282785	0.000038	0.0009	0.000009	0.0306	0.000412	258	0.5	6.0	1.4	660	820	-0.97
mpg-2-30	0.282747	0.000029	0.0013	0.000010	0.0456	0.000407	258	-0.9	4.6	1.2	722	900	-0.96



(a) 底图据 Hayashi 等 (1997) 与 He 等 (2014); (b) 底图据 Winchester 和 Floyd (1977); (c) 底图据 Pearce (1982); (d) 引自 Nesbitt 和 Young (1989)。峨眉山玄武岩数据引自 Xiao 等 (2004) 和 Xu 等 (2001), 峨眉山酸性火山岩数据引自 Cheng 等 (2017)、Xu 等 (2010) 和邵辉等 (2007), 宾川酸性熔结凝灰岩数据引自 Huang 等 (2018), 上二叠统峨眉山大火成岩省相关凝灰岩数据引自 Huang 等 (2018) 和 Zhong 等 (2020)。(d) 中 A 表示  $\text{Al}_2\text{O}_3$ , CN 表示  $(\text{CaO}^* + \text{Na}_2\text{O})$ , K 表示  $\text{K}_2\text{O}$ , CIA\* 表示钾交代作用之前的 CIA 值

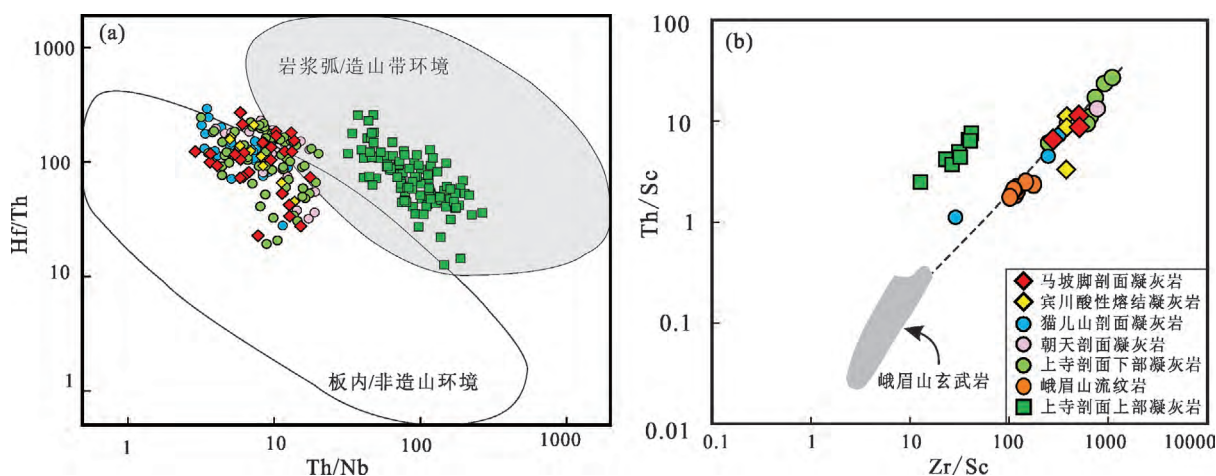
图 7 全岩主、微量元素  $\text{Al}_2\text{O}_3$ - $\text{TiO}_2$  图解(a)、 $\text{Nb}/\text{Y}$ - $\text{Zr}/\text{TiO}_2$  图解(b)、 $\text{Zr}$ - $\text{Ti}$  图解(c)和 A-CN-K 三角图(d)

Fig. 7 Diagrams of  $\text{Al}_2\text{O}_3$  vs.  $\text{TiO}_2$  (a),  $\text{Nb}/\text{Y}$  vs.  $\text{Zr}/\text{TiO}_2$  (b),  $\text{Zr}$  vs.  $\text{Ti}$  (c), and A-CN-K (d) of major elements of bulk rocks

2014; Liu et al., 2015)。岩浆弧成因火山岩在越南北部以及我国海南等地均有报道 (Li et al., 2006; Halpin et al., 2016)。锆石年龄为 255~252 Ma 的岩浆弧成因凝灰岩在宣城、煤山和上寺剖面上部的上二叠统地层中也见有报道 (He et al., 2014; Liao et al., 2016; Huang et al., 2018; Wang et al., 2019)。此外, 上寺剖面下部及猫儿山剖面还发育具有年龄为 260~257 M、形成于板内构造背景的凝灰岩 (Huang et al., 2018; Zhong et al., 2020)。相比于板内岩浆, 岩浆弧锆石具有相对高的 Th/Nb 值及较低的 Nb/Hf 值 (Yang et al., 2012)。锆石的 Th/Nb-Hf/Th 比值可用于区分岩浆的构造环境是板内(非造山带)还是岩浆弧(造山带) (Yang et al., 2012)。在锆石的 Th/Nb-Hf/Th 图(图 8a)中, 马坡

脚凝灰岩样品点均落入板内/非造山带区域。据此认为华南晚二叠世岩浆不是马坡脚凝灰岩的来源。

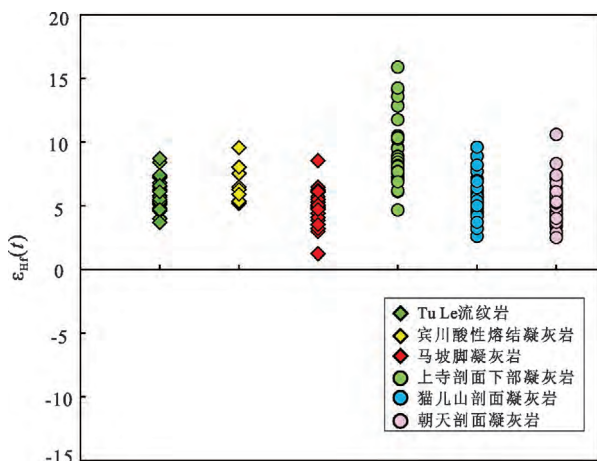
马坡脚凝灰岩与宾川熔结凝灰岩及峨眉山酸性火山岩有着近似的  $\text{Al}_2\text{O}_3/\text{TiO}_2$  比值(图 8a), 相似的球粒陨石标准化配分模式和原始地幔标准化微量元素特征(图 4)。在  $\text{Zr}/\text{Sc}-\text{Th}/\text{Sc}$  图(图 8b)中, 这些样品呈近似线性分布, 暗示其具有同源性。同时, 锆石微量元素显示马坡脚凝灰岩与宾川酸性熔结凝灰岩在均为板内/非造山构造环境。锆石 Hf 同位素分析结果显示, 马坡脚凝灰岩的锆石  $\varepsilon_{\text{Hf}}(t)$  值为 1.1~8.4, 表现地幔来源, 这与宾川酸性熔结凝灰岩 (Huang et al., 2018) 和 Tu Le 流纹岩 (Usuki et al., 2015) 的  $\varepsilon_{\text{Hf}}(t)$  值近似一致(图 9)。上寺剖面下部、朝天剖面及猫儿山剖面的凝灰岩都被证实来



(a) 底图据 Yang 等(2012)。数据来源:宾川酸性熔结凝灰岩和上寺凝灰岩据 Huang 等(2018);猫儿山剖面和朝天剖面凝灰岩据 Zhong 等(2020),张晗等(2020)。(b) 底图据 McLennan 等(1993)。数据来源:峨眉山流纹岩据 Xu 等(2010)和邵辉等(2007);宾川酸性熔结凝灰岩据 Huang 等(2018);猫儿山剖面凝灰岩据 Zhong 等(2020);朝天剖面凝灰岩据 Zhong 等(2020),张晗等(2020);上寺剖面凝灰岩据 Huang 等(2018)

图 8 锆石微量元素 Th/Nb-Hf/Th(a) 及全岩微量元素 Zr/Sc-Th/Sc(b) 图解

Fig. 8 Diagram of Th/Nb vs. Hf/Th (a) and Zr/Sc vs. Th/Sc (b) of zircons from various tuff samples



数据来源:宾川酸性熔结凝灰岩和上寺剖面下部的凝灰岩据 Huang 等(2018);Tu Le 流纹岩据 Usuki 等(2015);猫儿山剖面和朝天剖面据 Zhong 等(2020)

图 9 不同凝灰岩和流纹岩锆石  $\varepsilon_{\text{Hf}}(t)$  值

Fig. 9 The  $\varepsilon_{\text{Hf}}(t)$  values of zircons from various tuffs and rhyolite

自与峨眉山大火成岩省相关的酸性火山活动(Huang et al., 2018; Zhong et al., 2020; 张晗等, 2020)。马坡脚凝灰岩与这些凝灰岩具有相似的地球化学特征(图 7、8),暗示它们都可能是峨眉山大火成岩省相关的酸性火山活动的产物。综上所述,马坡脚凝灰岩应与峨眉山大火成岩省酸性岩浆活动有关。

#### 4.2 峨眉山大火成岩省的火山活动终止时限

由于峨眉山大火成岩省受到中-新生代复杂构

造热事件的影响,其 Ar-Ar 体系遭到破坏,故玄武岩 Ar-Ar 年龄常偏年轻(Lo et al., 2002; Ali et al., 2004, 2005)。传统的锆石 U-Pb 定年方法(SHRIMP 和 LA-ICP-MS)误差较大,可能大于火山活动本身的持续时间(徐义刚等, 2013; Zhong et al., 2014)。化学剥蚀热电离质谱(CA-TIMS)方法的锆石 U-Pb 定年精度优于 0.1%,远高于 SHRIMP 或 LA-ICP-MS 微区定年的 1%~2% 的精度(Mattinson, 2005; 李秋立, 2015)。Zhong 等(2014)利用 CA-TIMS 法测得峨眉山中心地区云南宾川剖面玄武岩顶部夹层中酸性熔结凝灰岩的高精度锆石 U-Pb 年龄为  $(259.1 \pm 0.5)$  Ma,认为其代表了峨眉山火山活动的终止年龄。Yang 等(2018)同样利用 CA-TIMS 技术在大火成岩省东部贵州普安剖面玄武岩顶部的凝灰岩测得了  $(259.51 \pm 0.21)$  Ma 的锆石年龄。

然而,现今峨眉山序列火山岩的锆石年龄能否约束峨眉山火山活动的终止时间尚存争议(Huang et al., 2018)。峨眉山火山岩与上覆上二叠统或下三叠统均呈不整合接触,二者之间存在沉积间断。同时,物源分析显示,峨眉山大火成岩省受到过强烈的风化侵蚀,其剥蚀产生的火山碎屑物质在大火成岩省周边的上二叠统和下三叠统地层中普遍存在(He et al., 2007; Dai et al., 2014; Huang et al., 2014, 2021; Yang et al., 2014; Yu et al., 2016; Deng et al., 2020)。因此,现存峨眉山火山序列可

能无法限制峨眉山火山活动的结束时间。

马坡脚剖面记录的碳酸盐岩台地沉降、碳同位素漂移和锶同位素比值降低,都被认为可能与峨眉山大火成岩省的火山活动有关(Bagherpour et al., 2018a, 2018b)。本次研究证实,马坡脚剖面的凝灰岩应来自与峨眉山大火成岩省相关的酸性火山活动。马坡脚剖面2个凝灰岩样品的高精度CA-TIMS年龄为( $258.4 \pm 0.11$ ) Ma和( $258.649 \pm 0.072$ ) Ma(Fortes De Lena, 2019),明显比宾川熔结凝灰岩和普安凝灰岩的年轻,暗示峨眉山大火成岩省的火山活动至少持续到了晚二叠世吴家坪早期。

#### 4.3 峨眉山大火成岩省的酸性火山活动与晚二叠世气候持续变冷事件关系

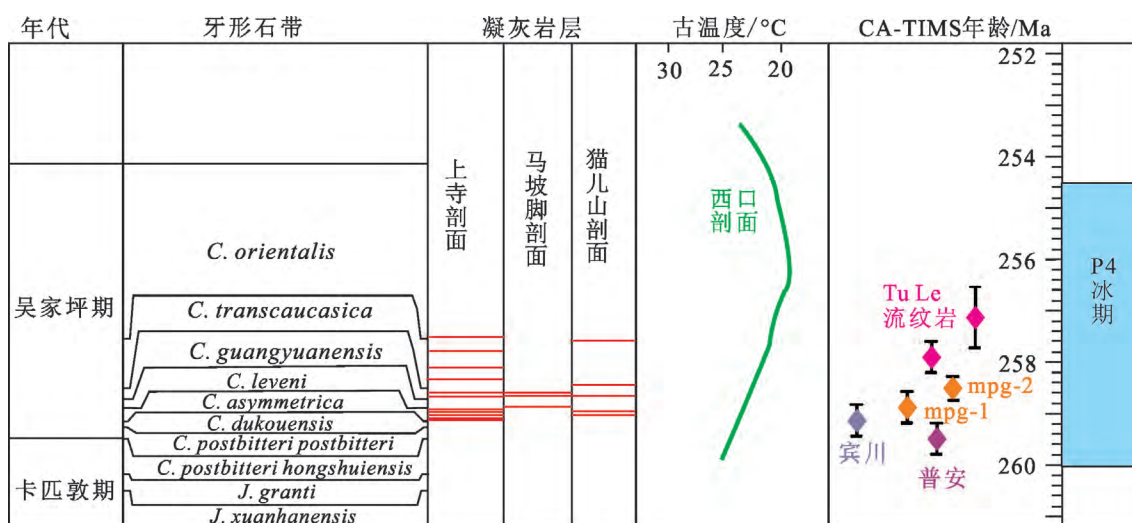
大火成岩省被普遍认为是促使全球环境剧变和生物灭绝的重要因素(Kidder and Worsley, 2010; Bond and Wignall, 2014; Mather, 2015; Ernst and Youbi, 2017; 徐义刚等, 2017)。地质历史时期,大火成岩省与冰期存在很好的时间耦合关系(Youbi et al., 2021)。二叠纪是全球气候由冰室向温室的转折期(Frank et al., 2015; 陈军和徐义刚, 2017)。澳大利亚东部地层记录显示,二叠纪共有四次独立的冰期事件(Fielding et al., 2008),其中二叠纪最末次冰期(P4冰期)的高精度年龄为260~254.5 Ma(Metcalfe et al., 2015)。在低纬度的华南地区,牙形石氧同位素记录显示,中晚二叠之交及吴家坪早期至吴家坪中期海水温度显著降低(Chen et al., 2011,

2013)。Wang等(2020)通过研究陕西西口剖面腕足动物壳体氧同位素组成,进一步证明吴家坪早期至吴家坪中期气候存在持续变冷的现象(图10)。

峨眉山玄武岩喷发后风化被认为是中晚二叠世之交气候变冷的影响因素之一(Yang et al., 2018)。然而,大火成岩省的酸性岩浆活动对气候的影响同样不可忽视。酸性火山活动释放大量CO<sub>2</sub>、SO<sub>2</sub>气体以及粉尘进入大气(Bryan et al., 2002; Self et al., 2006)。其中,SO<sub>2</sub>气体经火山喷发进入大气后,会转变为硫酸盐气溶胶,阻挡太阳辐射,进而引起气候变冷(Thordarson et al., 1996; Thordarson and Self, 2003; Ward, 2009)。马坡脚、猫儿山及上寺剖面下部分布的凝灰岩层暗示峨眉山酸性火山活动可能间歇性喷发至吴家坪中期(图10)。结合Shellnutt等(2020)对越南北部Tu Le流纹岩的研究,峨眉山酸性喷发规模可能是Yang等(2015)先前计算的两倍以上,共有超过 $4 \times 10^5$  Mt SO<sub>2</sub>被释放到大气中。大规模的SO<sub>2</sub>经间歇性、高频次的喷发进入大气,会形成持续性“火山冬天”气候,引发长期气候变冷(Zhang et al., 2013)。因此,峨眉山大火成岩省酸性岩浆的喷发规模可能数倍于先前的估算,其气候效应可能导致了吴家坪早期至吴家坪中期的气候变冷。

## 5 结论

(1) 马坡脚剖面上二叠统吴家坪组的凝灰岩来



数据来源:二叠纪地层框架及牙形石生物带年龄引自沈树忠等(2019);上寺剖面凝灰岩据 Huang 等(2018);猫儿山剖面据 Zhong 等(2020);宾川酸性熔结凝灰岩据 Zhong 等(2014);普安凝灰岩据 Yang 等(2018);Tu Le 流纹岩据 Shellnutt 等(2020);马坡脚凝灰岩对应的高精度年龄据 Fortes De Lena(2019);西口剖面腕足动物壳体氧同位素古温度数据引自 Wang 等(2020);P4 冰期年  
龄据 Metcalfe 等(2015)

图 10 峨眉山酸性火山活动与气候变冷事件

Fig. 10 The relationship between the Emeishan felsic volcanisms and climatic cooling events

自峨眉山大火成岩省的酸性火山活动。

(2) 峨眉山酸性火山活动可能至少延续至晚二叠世吴家坪早期。

(3) 峨眉山酸性火山喷发可能是吴家坪早期至吴家坪中期气候变冷的重要影响因素之一。

### 参考文献 (References):

- Ali J R, Lo C H, Thompson G M, Song X Y. 2004. Emeishan Basalt Ar-Ar overprint ages define several tectonic events that affected the western Yangtze platform in the Mesozoic and Cenozoic. *Journal of Asian Earth Sciences*, 23(2): 163–178
- Ali J R, Thompson G M, Zhou M F, Song X Y. 2005. Emeishan large igneous province, SW China. *Lithos*, 79(3–4): 475–489
- Ali J R, Fitton J G, Herzberg C. 2010. Emeishan large igneous province (SW China) and the mantle-plume up-doming hypothesis. *Journal of the Geological Society*, 167(5): 953–959
- Bagherpour B, Bucher H, Schneebeli-Hermann E, Vennemann T, Chiara M, Shen S Z. 2018a. Early Late Permian coupled carbon and strontium isotope chemostratigraphy from South China: Extended Emeishan volcanism? *Gondwana Research*, 58: 58–70
- Bagherpour B, Bucher H, Yuan D X, Leu M, Zhang C, Shen S Z. 2018b. Early Wuchiapingian (Lopingian, late Permian) drowning event in the South China block suggests a late eruptive phase of Emeishan large Igneous Province. *Global and Planetary Change*, 169: 119–132
- Blichert-Toft J, Albarède F. 1997. The Lu-Hf isotope geochemistry of chondrites and the evolution of the mantle-crust system. *Earth and Planetary Science Letters*, 148(1–2): 243–258
- Bond D P G, Wignall P B. 2014. Large igneous provinces and mass extinctions: An update. In: Keller G, Kerr A C, eds. *Volcanism, Impacts, and Mass Extinctions: Causes and Effects*. America: Geological Society of America, 29–55
- Bryan S E, Riley T R, Jerram D A, Stephens C J, Leat P T. 2002. Silicic volcanism: An undervalued component of large igneous provinces and volcanic rifted margins. In: Menzies M A, Klemperer S L, Ebinger C J, Baker J, eds. *Volcanic Rifted Margins*. America: Geological Society of America, 97–118
- Chen B, Joachimski M M, Sun Y D, Shen S Z, Lai X L. 2011. Carbon and conodont apatite oxygen isotope records of Guadalupian-Lopingian boundary sections: Climatic or sea-level signal? *Palaeogeography, Palaeoclimatology, Palaeoecology*, 311(3–4): 145–153
- Chen B, Joachimski M M, Shen S Z, Lambert L L, Lai X L, Wang X D, Chen J, Yuan D X. 2013. Permian ice volume and palaeoclimate history: Oxygen isotope proxies revisited. *Gondwana Research*, 24(1): 77–89
- Cheng L L, Wang Y, Herrin J S, Ren Z Y, Yang Z F. 2017. Origin of K-feldspar megacrysts in rhyolites from the Emeishan large igneous province, southwest China. *Lithos*, 294–295: 397–411
- Dai S F, Li T, Seredin V V, Ward C R, Hower J C, Zhou Y P, Zhang M Q, Song X L, Song W J, Zhao C L. 2014. Origin of minerals and elements in the Late Permian coals, tonsteins, and host rocks of the Xinde Mine, Xuanwei, eastern Yunnan, China. *International Journal of Coal Geology*, 121: 53–78
- Deng X S, Yang J H, Cawood P A, Wang X C, Du Y S, Huang Y, Lu S F, He B. 2020. Detrital record of late-stage silicic volcanism in the Emeishan large igneous province. *Gondwana Research*, 79: 197–208
- Ernst R E, Youbi N. 2017. How Large Igneous Provinces affect global climate, sometimes cause mass extinctions, and represent natural markers in the geological record. *Palaeogeography, Palaeoclimatology, Palaeoecology*, 478: 30–52
- Fedo C M, Wayne Nesbitt H, Young G M. 1995. Unraveling the effects of potassium metasomatism in sedimentary rocks and paleosols, with implications for paleoweathering conditions and provenance. *Geology*, 23(10): 921–924
- Fielding C R, Frank T D, Birgenheier L P, Rygel M C, Jones A T, Roberts J. 2008. Stratigraphic imprint of the Late Palaeozoic Ice Age in eastern Australia: A record of alternating glacial and nonglacial climate regime. *Journal of the Geological Society*, 165(1): 129–140
- Fortes De Lena L O. 2019. Establishing a robust timeframe for environmental change in the geological past through combined use of high-precision u-pb geochronology of zircon from volcanic ash layers and age-depth modelling. Doctoral Thesis. Genève: University of Genève
- Frank T D, Shultz A I, Fielding C R. 2015. Acme and demise of the late Palaeozoic ice age: A view from the southeastern margin of Gondwana. *Palaeogeography, Palaeoclimatology, Palaeoecology*, 418: 176–192
- Griffin W L, Pearson N J, Belousova E, Jackson S E, Van Achterbergh E, O’Reilly S Y, Shee S R. 2000. The Hf isotope composition of cratonic mantle: LAM-MC-ICPMS analysis of zircon megacrysts in kimberlites. *Geochimica et Cosmochimica Acta*, 64(1): 133–147
- Halpin J A, Tran H T, Lai C K, Meffre S, Crawford A J, Zaw K. 2016. U-Pb zircon geochronology and geochemistry from NE Vietnam: A ‘tectonically disputed’ territory between the Indochina and South China blocks. *Gondwana Research*, 34: 254–273
- Hayashi K I, Fujisawa H, Holland H D, Ohmoto H. 1997. Geochemistry of ~1.9 Ga sedimentary rocks from northeastern Labrador, Canada. *Geochimica et Cosmochimica Acta*, 61(19): 4115–4137
- He B, Xu Y G, Huang X L, Luo Z Y, Shi Y R, Yang Q J, Yu S Y. 2007. Age and duration of the Emeishan flood volcanism, SW China: Geochemistry and SHRIMP zircon U-Pb dating of silicic ignimbrites, post-volcanic Xuanwei Formation and clay tuff at the Chao-tian section. *Earth and Planetary Science Letters*, 255(3–4): 306–323
- He B, Zhong Y T, Xu Y G, Li X H. 2014. Triggers of Permo-Triassic boundary mass extinction in South China: The Siberian Traps or Paleo-Tethys ignimbrite flare-up? *Lithos*, 204: 258–267
- Hoskin P W O, Schaltegger U. 2003. The composition of zircon and igneous and metamorphic petrogenesis. *Reviews in Mineralogy and Geochemistry*, 53(1): 27–62
- Hu P Y, Li C, Li J, Wang M, Xie C M, Wu Y W. 2014. Zircon U-Pb–Hf isotopes and whole-rock geochemistry of gneissic granites from the Jitang complex in Leiwuqi area, eastern Tibet, China: Record of the

- closure of the Paleo-Tethys Ocean. *Tectonophysics*, 623: 83–99
- Hu Z C, Gao S, Liu Y S, Hu S H, Chen H H, Yuan H L. 2008. Signal enhancement in laser ablation ICP-MS by addition of nitrogen in the central channel gas. *Journal of Analytical Atomic Spectrometry*, 23(8): 1093–1101
- Hu Z C, Liu Y S, Gao S, Liu W G, Zhang W, Tong X R, Lin L, Zong K Q, Li M, Chen H H, Zhou L, Yang L. 2012a. Improved in situ Hf isotope ratio analysis of zircon using newly designed X skimmer cone and jet sample cone in combination with the addition of nitrogen by laser ablation multiple collector ICP-MS. *Journal of Analytical Atomic Spectrometry*, 27(9): 1391–1399
- Hu Z C, Liu Y S, Gao S, Xiao S Q, Zhao L S, Günther D, Li M, Zhang W, Zong K Q. 2012b. A “wire” signal smoothing device for laser ablation inductively coupled plasma mass spectrometry analysis. *Spectrochimica Acta Part B: Atomic Spectroscopy*, 78: 50–57
- Huang H, Du Y S, Yang J H, Zhou L, Hu L S, Huang H W, Huang Z Q. 2014. Origin of Permian basalts and clastic rocks in Napo, Southwest China: Implications for the erosion and eruption of the Emeishan large igneous province. *Lithos*, 208–209: 324–338
- Huang H, Cawood P A, Hou M C, Yang J H, Ni S J, Du Y S, Yan Z K, Wang J. 2016. Silicic ash beds bracket Emeishan large igneous province to < 1 m. y. at ~ 260 Ma. *Lithos*, 264: 17–27
- Huang H, Cawood P A, Hou M C, Ni S J, Yang J H, Du Y S, Wen H G. 2018. Provenance of Late Permian volcanic ash beds in South China: Implications for the age of Emeishan volcanism and its linkage to climate cooling. *Lithos*, 314–315: 293–306
- Huang H, Cawood P A, Hou M C, Xiong F H, Ni S J, Deng M, Zhong H T, Yang C C. 2021. Zircon U-Pb age, trace element, and Hf isotopic constraints on the origin and evolution of the Emeishan Large Igneous Province. *Gondwana Research*, doi: 10.1016/j.gr.2021.09.023
- Kidder D L, Worsley T R. 2010. Phanerozoic large igneous provinces (LIPs), HEATT (haline euxinic acidic thermal transgression) episodes, and mass extinctions. *Palaeogeography, Palaeoclimatology, Palaeoecology*, 295(1–2): 162–191
- Li X H, Li Z X, Li W X, Wang Y J. 2006. Initiation of the Indosinian orogeny in South China: Evidence for a Permian magmatic arc on Hainan Island. *The Journal of Geology*, 114(3): 341–353
- Liao Z W, Hu W X, Cao J, Wang X L, Yao S P, Wu H G, Wan Y. 2016. Heterogeneous volcanism across the Permian-Triassic Boundary in South China and implications for the Latest Permian Mass Extinction: New evidence from volcanic ash layers in the Lower Yangtze Region. *Journal of Asian Earth Sciences*, 127: 197–210
- Liu H C, Wang Y J, Cawood P A, Fan W M, Cai Y F, Xing X W. 2015. Record of Tethyan ocean closure and Indosinian collision along the Ailaoshan suture zone (SW China). *Gondwana Research*, 27(3): 1292–1306
- Liu Y S, Hu Z C, Gao S, Günther D, Xu J, Gao C G, Chen H H. 2008a. In situ analysis of major and trace elements of anhydrous minerals by LA-ICP-MS without applying an internal standard. *Chemical Geology*, 257(1–2): 34–43
- Liu Y S, Zong K Q, Kelemen P B, Gao S. 2008b. Geochemistry and magmatic history of eclogites and ultramafic rocks from the Chinese continental scientific drill hole: Subduction and ultrahigh-pressure metamorphism of lower crustal cumulates. *Chemical Geology*, 247(1–2): 133–153
- Liu Y S, Gao S, Hu Z C, Gao C G, Zong K Q, Wang D B. 2010a. Continental and Oceanic Crust Recycling-induced Melt-Peridotite Interactions in the Trans-North China Orogen: U-Pb Dating, Hf Isotopes and Trace Elements in Zircons from Mantle Xenoliths. *Journal of Petrology*, 51(1–2): 537–571
- Liu Y S, Hu Z C, Zong K Q, Gao C G, Gao S, Xu J, Chen H H. 2010b. Reappraisal and refinement of zircon U-Pb isotope and trace element analyses by LA-ICP-MS. *Chinese Science Bulletin*, 55(15): 1535–1546
- Lo C H, Chung S L, Lee T Y, Wu G Y. 2002. Age of the Emeishan flood magmatism and relations to Permian-Triassic boundary events. *Earth and Planetary Science Letters*, 198(3–4): 449–458
- Ludwig K R. 2003. ISOPLOT 3.00: A geochronological toolkit for Microsoft Excel. California: Berkeley Geochronology Center, 1–70
- Mather T A. 2015. Volcanoes and the environment: Lessons for understanding Earth’s past and future from studies of present-day volcanic emissions. *Journal of Volcanology and Geothermal Research*, 304: 160–179
- Mattinson J M. 2005. Zircon U-Pb chemical abrasion (“CA-TIMS”) method: combined annealing and multi-step partial dissolution analysis for improved precision and accuracy of zircon ages. *Chemical Geology*, 220(1–2): 47–66
- McLennan S M, Hemming S, McDaniel D K, Hanson G N. 1993. Geochemical approaches to sedimentation, provenance, and tectonics. In: Johnsson M J, Basu A, eds. *Processes Controlling the Composition of Clastic Sediments*. America: Geological Society of America, 21
- Metcalfe I, Crowley J L, Nicoll R S, Schmitz M. 2015. High-precision U-Pb CA-TIMS calibration of Middle Permian to Lower Triassic sequences, mass extinction and extreme climate-change in eastern Australian Gondwana. *Gondwana Research*, 28(1): 61–81
- Mundil R, Ludwig K R, Metcalfe I, Renne P R. 2004. Age and timing of the Permian mass extinctions: U/Pb dating of closed-system zircons. *Science*, 305(5691): 1760–1763
- Nesbitt H W, Young G M. 1982. Early Proterozoic climates and plate motions inferred from major element chemistry of lutites. *Nature*, 299(5885): 715–717
- Nesbitt H W, Young G M. 1989. Formation and diagenesis of weathering profiles. *The Journal of Geology*, 97(2): 129–147
- Pearce J A. 1982. Trace element characteristics of lavas from destructive plate boundaries. In: Thorpe R S, ed. *Andesites, Orogenic Andesites and Related Rocks*. Chichester: Wiley, 528–548
- Scherer E, Müunker C, Mezger K. 2001. Calibration of the lutetium-hafnium clock. *Science*, 293(5530): 683–687
- Self S, Widdowson M, Thordarson T, Jay A E. 2006. Volatile fluxes during flood basalt eruptions and potential effects on the global environment: A Deccan perspective. *Earth and Planetary Science Letters*, 248(1–2): 518–532
- Shellnutt J G, Jahn B M, Zhou M F. 2011. Crustally-derived granites in the Panzhihua region, SW China: Implications for felsic magmatism in the

- Emeishan large igneous province. *Lithos*, 123(1-4): 145-157
- Shellnutt J G. 2014. The Emeishan large igneous province: A synthesis. *Geoscience Frontiers*, 5(3): 369-394
- Shellnutt J G, Pham T T, Denysyn S W, Yeh M W, Tran T A. 2020. Magmatic duration of the Emeishan large igneous province: Insight from northern Vietnam. *Geology*, 48(5): 457-461
- Shen S Z, Henderson C M, Bowring S A, Cao C Q, Wang Y, Wang W, Zhang H, Zhang Y C, Mu L. 2010. High - resolution Lopingian (Late Permian) timescale of south China. *Geological Journal*, 45(2-3): 122-134
- Shen S Z, Crowley J L, Wang Y, Bowring S A, Erwin D H, Sadler P M, Cao C Q, Rothman D H, Henderson C M, Ramezani J, Zhang H, Shen Y N, Wang X D, Wang W, Mu L, Li W Z, Tang Y G, Liu X L, Liu L J, Zeng Y, Jiang Y F, Jin Y G. 2011. Calibrating the end-Permian mass extinction. *Science*, 334 ( 6061 ): 1367-1372
- Sun S S, McDonough W F. 1989. Chemical and isotopic systematics of oceanic basalts: Implications for mantle composition and processes. Geological Society, London, Special Publications, 42: 313-345
- Sun Y D, Lai X L, Wignall P B, Widdowson M, Ali J R, Jiang H S, Wang W, Yan C B, Bond D P G, Védrine S. 2010. Dating the onset and nature of the Middle Permian Emeishan large igneous province eruptions in SW China using conodont biostratigraphy and its bearing on mantle plume uplift models. *Lithos*, 119(1-2): 20-33
- Thordarson T, Self S, Óskarsson N, Hulsebosch T. 1996. Sulfur, chlorine, and fluorine degassing and atmospheric loading by the 1783-1784 AD Laki (Skaftár Fires) eruption in Iceland. *Bulletin of Volcanology*, 58(2): 205-225
- Thordarson T, Self S. 2003. Atmospheric and environmental effects of the 1783-1784 Laki eruption: A review and reassessment. *Journal of Geophysical Research: Atmospheres*, 108(D1): 4011
- Usuki T, Lan C Y, Tran T H, Pham T D, Wang K L, Shellnutt G J, Chung S L. 2015. Zircon U-Pb ages and Hf isotopic compositions of alkaline silicic magmatic rocks in the Phan Si Pan-Tu Le region, northern Vietnam: Identification of a displaced western extension of the Emeishan Large Igneous Province. *Journal of Asian Earth Sciences*, 97: 102-124
- Wang W Q, Garbelli C, Zhang F F, Zheng Q F, Zhang Y C, Yuan D X, Shi Y K, Chen B, Shen S Z. 2020. A high-resolution Middle to Late Permian paleotemperature curve reconstructed using oxygen isotopes of well-preserved brachiopod shells. *Earth and Planetary Science Letters*, 540: 116245
- Wang X D, Cawood P A, Zhao L S, Chen Z Q, Lyu Z, Ma B. 2019. Convergent continental margin volcanic source for ash beds at the Permian-Triassic boundary, South China: Constraints from trace elements and Hf-isotopes. *Palaeogeography, Palaeoclimatology, Palaeoecology*, 519: 154-165
- Ward P L. 2009. Sulfur dioxide initiates global climate change in four ways. *Thin Solid Films*, 517(11): 3188-3203
- Wiedenbeck M, Allé P, Corfu F, Griffin W L, Meier M, Oberli F, Von Quadt A, Roddick J C, Spiegel W. 1995. Three natural zircon standards for U-Th-Pb, Lu-Hf, trace element and REE analyses. *Geostandards Newsletter*, 19(1): 1-23
- Winchester J A, Floyd P A. 1977. Geochemical discrimination of different magma series and their differentiation products using immobile elements. *Chemical Geology*, 20: 325-343
- Xiao L, Xu Y G, Mei H J, Zheng Y F, He B, Pirajno F. 2004. Distinct mantle sources of low-Ti and high-Ti basalts from the western Emeishan large igneous province, SW China: Implications for plume-lithosphere interaction. *Earth and Planetary Science Letters*, 228 ( 3-4 ): 525-546
- Xu Y G, Chung S L, Jahn B M, Wu G Y. 2001. Petrologic and geochemical constraints on the petrogenesis of Permian-Triassic Emeishan flood basalts in southwestern China. *Lithos*, 58 ( 3-4 ): 145-168
- Xu Y G, Luo Z Y, Huang X L, He B, Xiao L, Xie L W, Shi Y R. 2008. Zircon U-Pb and Hf isotope constraints on crustal melting associated with the Emeishan mantle plume. *Geochimica et Cosmochimica Acta*, 72(13): 3084-3104
- Xu Y G, Chung S L, Shao H, He B. 2010. Silicic magmas from the Emeishan large igneous province, Southwest China: Petrogenesis and their link with the end-Guadalupian biological crisis. *Lithos*, 119(1-2): 47-60
- Yang J H, Cawood P A, Du Y S, Huang H, Huang H W, Tao P. 2012. Large Igneous Province and magmatic arc sourced Permian-Triassic volcanogenic sediments in China. *Sedimentary Geology*, 261-262: 120-131
- Yang J H, Cawood P A, Du Y S, Huang H, Hu L S. 2014. A sedimentary archive of tectonic switching from Emeishan Plume to Indosian orogenic sources in SW China. *Journal of the Geological Society*, 171(2): 269-280
- Yang J H, Cawood P A, Du Y S. 2015. Voluminous silicic eruptions during late Permian Emeishan igneous province and link to climate cooling. *Earth and Planetary Science Letters*, 432: 166-175
- Yang J H, Cawood P A, Du Y S, Condon D J, Yan J X, Liu J Z, Huang Y, Yuan D X. 2018. Early Wuchiapingian cooling linked to Emeishan basaltic weathering? *Earth and Planetary Science Letters*, 492: 102-111
- Youbi N, Ernst R E, Mitchell R N, Boumehdi M A, El Moume W, Lahna A A, Bensalah M K, Söderlund U, Doblas M, Tassinari C C G. 2021. Preliminary appraisal of a correlation between glaciations and large igneous provinces over the past 720 million years. In: Ernst R E, Dickson A J, Bekker A, eds. *Large Igneous Provinces: A Driver of Global Environmental and Biotic Changes*. New York: AGU, 169-190
- Yu W C, Algeo T J, Du Y S, Zhang Q L, Liang Y P. 2016. Mixed volcanogenic-lithogenic sources for Permian bauxite deposits in southwestern Youjiang Basin, South China, and their metallogenic significance. *Sedimentary Geology*, 341: 276-288
- Zhang Y, Ren Z Y, Xu Y G. 2013. Sulfur in olivine - hosted melt inclusions from the Emeishan picrites: Implications for S degassing and its impact on environment. *Journal of Geophysical Research: Solid Earth*, 118(8): 4063-4070
- Zheng L D, Yang Z Y, Tong Y B, Yuan W. 2010. Magnetostriatigraphic constraints on two - stage eruptions of the Emeishan continental flood basalts. *Geochemistry, Geophysics, Geosystems*, 11

(12) : Q12014

Zhong Y T, He B, Mundil R, Xu Y G. 2014. CA-TIMS zircon U-Pb dating of felsic ignimbrite from the Binchuan section: Implications for the termination age of Emeishan large igneous province. *Lithos*, 204: 14–19

Zhong Y T, Mundil R, Chen J, Yuan D X, Denyszyn S W, Jost A B, Payne J L, He B, Shen S Z, Xu Y G. 2020. Geochemical, biostratigraphic, and high-resolution geochronological constraints on the waning stage of Emeishan Large Igneous Province. *GSA Bulletin*, 132(9–10): 1969–1986

Zhou M F, Malpas J, Song X Y, Robinson P T, Sun M, Kennedy A K, Lesher C M, Keays R R. 2002. A temporal link between the Emeishan large igneous province (SW China) and the end-Guadalupian mass extinction. *Earth and Planetary Science Letters*, 196(3–4): 113–122

Zhou M F, Robinson P T, Lesher C M, Keays R R, Zhang C J, Malpas J. 2005. Geochemistry, petrogenesis and metallogenesis of the Panzhihua gabbroic layered intrusion and associated Fe-Ti-V oxide deposits, Sichuan Province, SW China. *Journal of Petrology*, 46(11): 2253–2280

Zhou M F, Zhao J H, Qi L, Su W C, Hu R Z. 2006. Contributions to Mineralogy and Petrology, 151(1): 1–19

Zhu D C, Mo X X, Niu Y L, Zhao Z D, Wang L Q, Pan G T, Wu F Y. 2009. Zircon U-Pb dating and in-situ Hf isotopic analysis of Permian peraluminous granite in the Lhasa terrane, southern Tibet: Implications for Permian collisional orogeny and paleogeography. *Tectono-*

*physics*, 469(1–4): 48–60

Zi J W, Cawood P A, Fan W M, Tohver E, Wang Y J, McCuaig T C, Peng T P. 2013. Late Permian-Triassic magmatic evolution in the Jinshajiang orogenic belt, SW China and implications for orogenic processes following closure of the Paleo-Tethys. *American Journal of Science*, 313(2): 81–112

陈军, 徐义刚. 2017. 二叠纪大火成岩省的环境与生物效应: 进展与前瞻. *矿物岩石地球化学通报*, 36(3): 374–393

李秋立. 2015. U-Pb 定年体系特点和分析方法解析. *矿物岩石地球化学通报*, 34(3): 491–500

邵辉, 徐义刚, 何斌, 黄小龙, 罗震宇. 2007. 峨眉山大火成岩省晚期酸性火山岩的岩石地球化学特征. *矿物岩石地球化学通报*, 26(4): 350–358

沈树忠, 张华, 张以春, 袁东勋, 陈波, 何卫红, 牟林, 林巍, 王文倩, 陈军, 吴琼, 曹长群, 王玥, 王向东. 2019. 中国二叠纪综合地层和时间框架. *中国科学: 地球科学*, 49(1): 160–193

徐义刚, 何斌, 罗震宇, 刘海泉. 2013. 我国大火成岩省和地幔柱研究进展与展望. *矿物岩石地球化学通报*, 32(1): 25–39

徐义刚, 钟玉婷, 位荀, 陈军, 刘海泉, 颜炜, 罗震宇, 李洪颜, 何斌, 黄小龙, 王焰, 陈赟. 2017. 二叠纪地幔柱与地表系统演变. *矿物岩石地球化学通报*, 36(3): 359–373

张晗, 黄虎, 侯明才. 2020. 四川广元地区朝天剖面上二叠统吴家坪组凝灰岩成因及其地质意义. *地球科学与环境学报*, 42(1): 36–48

(本文责任编辑:龚超颖;英文审校:张兴春)